Towards real time monitoring of reacting species and pH coupling electrical resistance tomography and machine learning methodologies

Towards real time monitoring of reacting species and pH coupling Electrical Resistance Tomography and machine learning methodologies.

F.Alberini[1,#], D.Bezchi[1], I.C. Mannino[2], A. Paglianti[3], G.Montante[2]

[1] School of Chemical Engineering, University of Birmingham, Edgbaston Campus, B152TT, UK.
[2] Dipartimento di Chimica Industriale "Toso Montanari, Università di Bologna, viale Risorgimento 4, 40136, Bologna, Italy
[3] Dipartimento di Ingegneria Civile, Chimica, Ambientale e dei Materiali, Università di Bologna, via Terracini 34, 40131 Bologna, Italy
[#] Corresponding author: f.alberini@bham.ac.uk

Abstract

The development of smart sensors capable to analyse data gathered on the process line and to give a real time feedback has been undergoing extensive research in the last years due to its potential benefits on the process optimisation and products improvement. In this paper, a novel approach to detect and monitor pH and conductivity using 2D Electrical resistance Tomography (ERT) is proposed for the first time in a reacting system. As a study case, the reaction between phosphoric acid and potassium hydroxide in mediums of both water and sodium carboxymethylcellulose (CMC) aqueous solution was assessed. The information gathered using the ERT have been used to determine local and overall mixing time for a sequence of injections of base and acid to understand the overall performance of the system. In addition, the same information have been used to extrapolate live data about the variation of the pH coupling the ERT data and machine learning techniques. Three different approaches have been investigated to achieve the aforementioned objective all integrating ML to the data processing. The first two approaches did not provide satisfying results showing the limitation of a completely blind approach (pure statistical approaches). However, the last approach, which combined ML technique and physical/chemical knowledge, showed very successful results for the real time monitoring of the pH in a reacting system.

Keywords: mixing, electrical resistance tomography, pH, machine learning, reaction.

1.0 Introduction

Electrical resistance tomography (ERT) is an imaging technique which is often applied for geophysical subsurface analysis including mineral prospecting, hydrological exploration and environmental investigation. The imaging is determined by the characterisation of sub-surface materials by their electrical properties; electrodes are positioned appropriately and current is injected, with the resulting resistivity measured. As resistivity is the inverse of conductivity, the conductivity is then determined. In addition, there are numerous aqueous-based processes in which ERT is applied (Barber & Brown, 1983; Dickin & Wang, 1996).

As for the application in the chemical engineering field, in the last decades ERT has been employed for the investigation of several important industrial operations including mixing and multiphase flows (Sharifi & Young, 2013)and it was shown to be particularly suitable also for in-line process monitoring of mixing processes (Bowler et al., 2020). Among others, miscible and immiscible liquid/liquid mixing (Khajeh Naeeni & Pakzad, 2019; Maluta et al., 2020), mixing of non-Newtonian fluids (Kazemzadeh et al., 2016), solid/liquid mixing (Carletti et al., 2014; Hosseini et al., 2010), gas/liquid mixing (Montante

& Paglianti, 2015), gas/solid/liquid mixing (Forte, Alberini, et al., 2019) have been extensively investigated, as recently reviewed by Bowler et al. (2020). Comparatively the number of investigations that have concerned reactive systems with ERT, so far, are very limited. One of the first applications to the investigation of mixing with chemical reaction by ERT was proposed by Wabo et al. (2004). Afterwards, a few investigations on mixing and reactive precipitation of barium sulphate from barium chloride and sodium sulphate based on ERT have been carried out, going from the first demonstrative example of application (Kagoshima & Mann, 2005), to the quantification of the effect of the interaction between mixing and chemical reaction on the size and morphology of crystals (Gradov et al., 2018). Also, ERT was adopted in combination of Positon Emission Particle Tracking for the simultaneous investigation of hydrodynamics and precipitation of aluminium hydroxide (Edwards et al., 2009).

Overall, as a difference with non-reactive mixing, the amount of literature that covers reactive mixing investigations by ERT is very limited. Specifically, there is very little about monitoring of reactions in liquid medium using ERT and neither as potential tool to measure pH.

Although pH is a useful value for characterizing starter activity, pH probes are often unstable, and their calibration and maintenance are difficult. Electrical conductivity probes, which are more robust, can be used to monitor chemical variations, for example during a fermentation they have been proved to be effective (St-Gelais et al., 1995). However, only relying on the raw conductivity data, it could be challenging to differentiate different chemical formed species (it can happen that different species could increase the conductivity despite their different ion strength). This is why pH information is important as well to keep track of changes in a reacting system. Indeed, this is particularly true for single or parallel reactions monitoring (Rauniyar, 2015), which is a challenging requirement in particular during manufacturing. Commonly, mass spectrometry (Shi et al., 2012) is the standard tool which is used to track the progress of reactions, but mostly at R&D stage. Indeed, often the high costs of such equipment and its time scale of measurement limited its use at manufacturing stage (Bantscheff et al., 2007). In light of this, the research carried out in this work presents a new approach and methodology to monitor a reaction in a liquid medium using ERT.

This work is line with the basic concepts of the 4th Industrial revolution, where the ability to utilise techniques such as machine learning (ML) for the collection, processing, and evaluation of data on-demand is becoming increasingly significant.

Despite the use of artificial intelligence (AI) in chemical engineering is not new, it is, in fact, a 35-year-old ongoing program with some remarkable successes along the way, it is quite understandable that many chemical engineers are excited about the potential applications of AI. It might seem that this prospect offers a novel approach to challenging, long-standing problems in chemical engineering using AI (Venkatasubramanian, 2019). Machine learning is an interdisciplinary area, involving probability theory, statistics, approximation theory, convex analysis, algorithm complexity theory, and other disciplines. It is the core subset of artificial intelligence (AI). One of the advantages of ML approach is that the developed algorithms can build a mathematical model based on training data for predictions or decisions without being explicitly programmed to do so (Jiao et al., 2020). Machine learning has recently gained in popularity, spurred by well-publicized advances like deep learning and widespread commercial interest in big data analytics (Lee et al., 2018). As the number of data samples increases, the algorithm improves its performance. This learning can then be used to analyse a new set of data to draw conclusions from it (Parmar et al., 2015).

Although there is no precise definition of big data, it usually refers to the size and variety of datasets that challenge the ability of traditional processing and analytical tools to capture, store, manage, and analyse(Qin & Chiang, 2019).

Generally, machine learning is divided into supervised and unsupervised learning. Supervised machine learning is conducted with known input and output data to train the algorithm, whereas unsupervised learning has no specified output data. For this study, only supervised machine learning has been used, with particular attention to the regression learner applications. Regression is generally used to predict numerical, continuous responses. It uses one or several sets of data input, along with the corresponding output, and then maps a function to predict future outputs using new input data (Clarke et al., 2005; Rasmussen & De, 2010; Sheeba et al., 2020;)Hastie et al., n.d.).

In more detail, the objective of this study is to use the analytical information provided by ERT coupled with machine learning techniques to track a series of parallel reactions and their products. The experimental data have been collected from a series of experiments where phosphoric acid (H_3PO_4) and potassium hydroxide (KOH) were reacted together in a stirred vessel with incremental injections of each species using two different mediums. During the experiments, an independent measurement of pH as well as the conductivity of the solutions were taken using a pH-meter and a conductivity-meter respectively. Indeed, the final aim of this work was to demonstrate how supervised machine learning coupled with ERT data can provide information about the reaction developments. Thus, this will convert ERT as real-time monitoring tool for pH and species concentrations.

2.0 Material and methods

Experimental rig and procedure

The series of experiments were carried using a 6 L vessel, of diameter, T, equal to 20 cm, equipped with a Rushton Turbine of diameter, D, equal to T/3 located at the off-bottom clearance, C, equal to ~T/3 (see Figure 1), as schematically depicted in Figure 1. The impeller speed, N, was kept constant for all experiment at 150 rpm. The vessel was also equipped with two planes (see Figure 1A) of 16 electrodes connected to a four-channel V5R Data Acquisition System (DAS) supplied by Industrial Tomography System. The liquid height used was H=T which ensure to have enough liquid above the top measurement plane.

The electrodes were configured in a circular array around the periphery of the vessel (completely non-intrusive, the electrodes are mounted inside the wall of the tank), resulting in two separate measurement planes: Plane 1 was situated nearer the surface of the liquid (approximately 13.3 cm), while plane 2 was close the bottom of the vessel (6.7 cm). The size of each electrode was 20 mm by 20 mm .The device recorded conductivity values for 125 frames per second over the two planes, being the acquisition frequency equal to 62.5 Hz, with a total of 316 pixels in each plane. The acquisition voltage was set to 5V and the current amplitude was equal to 1.18 mA. As ERT is a non-invasive technique, it did not interfere with the reaction in any way (Forte, et al., 2019).

Two different fluids have been used: water and water with 0.2 wt.% carboxymethylcellulose (CMC). For each fluid, a reference was taken and in both cases the temperature was monitored with a standard conductivity meter probe, which had implemented a thermocouple as well. The probe was located (see Figure 1A and B, (1)) approximately in the middle between the shaft and the wall just above the top plane of the ERT to avoid any interference with it. On the opposite position (on the

cross section plane of the vessel) at same height, a pH meter was located as well (see Figure 1A and B, (3)). The experiments were carried out at temperature of approximately 20°C±0.5. The rheological model of the CMC solution was found to fit a power law model, as expected, and the rheological parameters associated to it. Consistency index, K, and power law number, n, where found to be 0.59 Pa s^n and 0.731 respectively (Stamatopoulos et al., 2015). The rheological measurements were carried out using a TA discovery hybrid rheometer (HR-1) equipped with a cone and plate stain steel geometry with 2° angle and a 52μm truncation gap. A steady state logarithmic (10 points per decade) flow ramp from 0.1 up to 350 s^{-1} was used to identify the rheological behaviour of the solution.

The choice of the different fluids was driven by the will of exploring two different flow regimes within the mixing vessel. To estimate those, both values of Reynolds number, Re, have been estimated using the standard definition of the rotational Reynolds number, using the same value of density equal to 1000 kg m^{-3}. For water, the viscosity of the medium is 0.001 Pa s and for CMC solution, the apparent viscosity (K $\bar{\gamma}^n/\bar{\gamma}$) has been calculated using the Metzger Otto method. This is based on the estimation of the average shear in the vessel, $\bar{\gamma}$= k_s N, where the constant k_s is taken equal to 11.5 for a Rushton turbine.

For the purpose of convenience, the first experiment is referred to as water, the second as CMC. At first, 6 injections of 81 wt.% phosphoric acid were added. This began with 1 ml added initially and then either 3 or 4 ml in each injection after, resulting in a total of 17 ml added. This was followed by injections of 25 wt.% potassium hydroxide, each being 3 ml, with 28 injections for water and 35 for CMC, resulting in a total of 34 and 41 injections for water and CMC, respectively. The time between each injection was selected based on live data. When the mean value of the conductivity and the standard deviation had a fairly constant flat profile, it was assumed that the system reached a steady state and the following injection was done. Each injection was done on the top of the vessel approximately in the perpendicular position respect to the conductivity and pH meters within the cross section of the vessel (see Figure 1B, (4)).

After each injection, the pH (accuracy 0.2) of the solution was measured, as well as the conductivity from the conductivity meter (accuracy 0.05 μS cm^{-1}) and from the ERT. The choice of measuring twice the conductivity was driven by the need of recording absolute steady state changes in the solutions (this done using a standard conductivity meter) as well as the conductivity changes throughout the whole duration of the experiment using the electrical resistance tomography (transient data with a time resolution of 1/62.5 second, ERT). Another feature, that has been determined using the transient data, was the mixing times for each injection. As mentioned, the pH was monitored as well to obtain a reference measurement to compare with the final results. The ERT, as well as providing data after each injection, was also monitoring the reaction throughout the whole course of the experiment, providing conductivity data for each pixel on a continuous basis. The ERT data were collected for both reactions mediums, and this was further subdivided into two planes, resulting in four sets of ERT data.

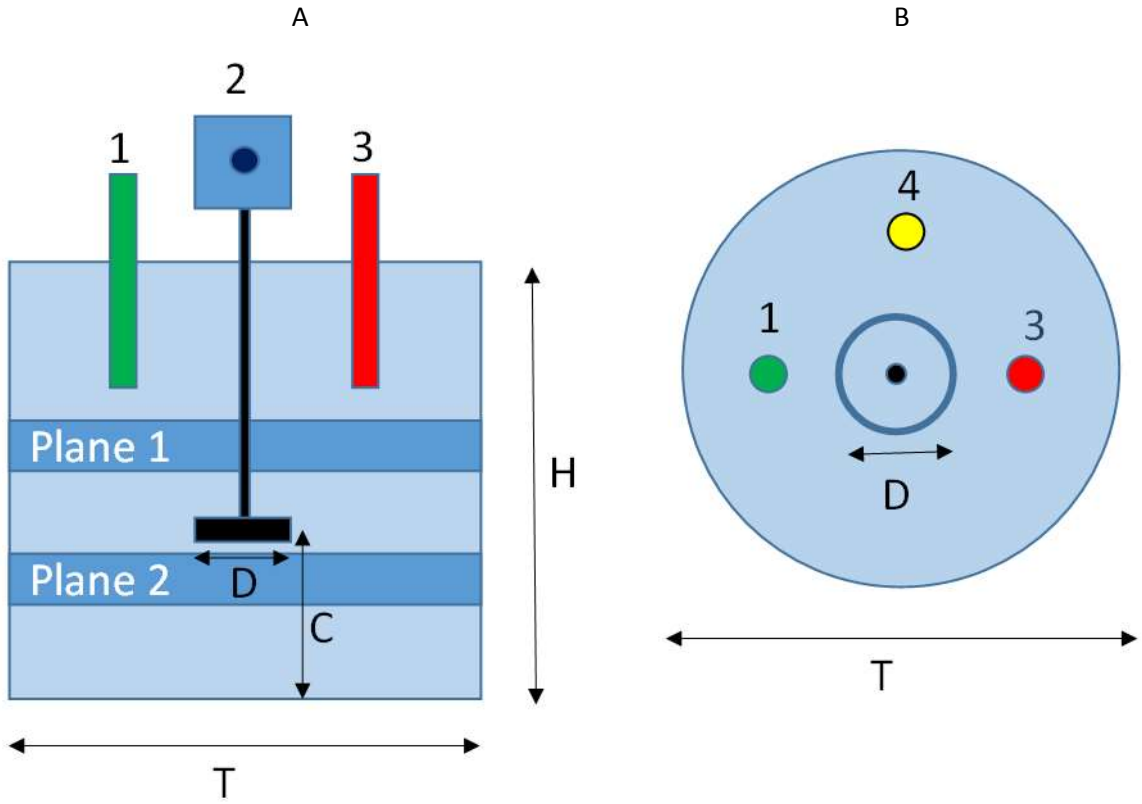

Figure 1. Schematic rig of the mixing vessel and locations of ERT Planes, conductivity meter (1), overhead mixer (2), pH meter (3) and injection position (4) for the side view (A) and cross section (B) as well.

Phosphoric acid and potassium hydroxide chemical reaction

The reaction between phosphoric acid and potassium hydroxide is summarised as follows:

$$H_3PO_4 + 3KOH \rightarrow K_3PO_4 + 3H_2O \quad (1)$$

Despite the presence of only four species in the reaction equation, there are also the dissociations of H_3PO_4 and KOH occurring. H_3PO_4 undergoes three dissociations:

$$H_3PO_4 \rightarrow H_2PO_4^- + H^+ \qquad K_{a1} = 6.9 \cdot 10^{-3} \quad (2)$$

$$H_2PO_4^- \rightarrow HPO_4^{2-} + H^+ \qquad K_{a2} = 6.2 \cdot 10^{-8} \qquad (3)$$

$$HPO_4^{2-} \rightarrow PO_4^{3-} + H^+ \qquad K_{a3} = 4.8 \cdot 10^{-13} \qquad (4)$$

The ionisation constant, K_a, values represent the degree to which dissociation occurs. It is the ratio of the concentration of the dissociated products to the concentration of the original species, for K_{a1}:

$$K_{a1} = \frac{[H^+][H_2PO_4^-]}{[H_3PO_4]} \qquad (5)$$

From the three acid dissociation equations and using data from the experiments, the molar fractions and molar concentrations of each species can be determined.

Rearranging the three acid dissociation equations:

$$[H^+] \cdot [H_2PO_4^-] = K_{a1} \cdot [H_3PO_4] \qquad (6)$$

$$[H^+] \cdot [HPO_4^{2-}] = K_{a2} \cdot [H_2PO_4^-] \qquad (7)$$

$$[H^+] \cdot [PO_4^{3-}] = K_{a3} \cdot [HPO_4^{2-}] \qquad (8)$$

The self-ionisation constant of water, K_w, is given by:

$$K_w = [H^+] \cdot [OH^-] = 1 \cdot 10^{-14} \qquad (9)$$

A molar balance on the total amount of phosphate gives:

$$[H_3PO_4] + [H_2PO_4^-] + [HPO_4^{2-}] + [PO_4^{3-}] = C \qquad (10)$$

Where C is the initial concentration of undissociated H_3PO_4.

The molar fraction a_x of each species is defined as:

$$a_x = \frac{[H_xPO_4]}{C} \qquad (11)$$

From this, it can be shown that:

$$\frac{1}{a_3} = \frac{C}{[H_3PO_4]} \qquad (12)$$

$$\frac{1}{a_3} = 1 + \frac{[H_2PO_4^-]}{[H_3PO_4]} + \frac{[HPO_4^{2-}]}{[H_3PO_4]} + \frac{[PO_4^{3-}]}{[H_3PO_4]} \qquad (13)$$

From (6):

$$\frac{[H_2PO_4^-]}{[H_3PO_4]} = \frac{K_{a1}}{[H^+]} \qquad (14)$$

Multiplying (6) and (7):

$$\frac{[HPO_4{}^{2-}]}{[H_3PO_4]} = \frac{K_{a1} \cdot K_{a2}}{[H^+]^2} \quad (15)$$

Multiplying (6), (7) and (8):

$$\frac{[PO_4{}^{3-}]}{[H_3PO_4]} = \frac{K_{a1} \cdot K_{a2} \cdot K_{a2}}{[H^+]^3} \quad (16)$$

Substituting (14), (15) and (16) into (13):

$$a_3 = \frac{1}{1 + \frac{K_{a1}}{[H^+]} + \frac{K_{a1} \cdot K_{a2}}{[H^+]^2} + \frac{K_{a1} \cdot K_{a2} \cdot K_{a2}}{[H^+]^3}} \quad (17)$$

By combining Eqns (6)-(8), (12), (18)-(19) and rearranging:

$$a_2 = \frac{a_3 \cdot K_{a1}}{[H^+]} \quad (18)$$

$$a_1 = \frac{a_3 \cdot K_{a1} \cdot K_{a2}}{[H^+]^2} \quad (19)$$

$$a_0 = \frac{a_3 \cdot K_{a1} \cdot K_{a2} \cdot K_{a2}}{[H^+]^3} \quad (20)$$

Thus, the concentration of the species derived from the dissociation of H_3PO_4 can be expressed by Eq. (11) as:

$$[H_xPO_4] = a_x \cdot C \quad (21)$$

Being the solution electrically neutral, the concentration of K^+ ions is found through:

$$[K^+] = [OH^-] - [H^+] + [H_2PO_4{}^-] + 2 \cdot [HPO_4{}^{2-}] + 3 \cdot [PO_4{}^{3-}] \quad (22)$$

The concentration of H^+ ions can be found from the pH:

$$[H^+] = 10^{-pH} \quad (23)$$

The concentration of OH^- ions can be subsequently found:

$$[OH^-] = \frac{K_w}{[H^+]} = \frac{1 \cdot 10^{-14}}{[H^+]} \quad (24)$$

Analytical data

The measured values for the water and CMC experiments at each injection have been recorded in time. In the supplementary information (SI) section the data are shown in Table 1.SI and 2.SI. The tables show the total cumulative amount of acid and base added after each injection, the pH of the solution, the specific conductivity measured by the conductivity meter and the average relative conductivity measured by ERT.

The concentration of acid, C, before the base addition was determined by multiplying the total amount of acid added (17 ml) by its molar concentration of 15.54 mol dm^{-3}, which was determined from its mass fraction of 81 wt.%, and then dividing by the total fluid volume in the vessel, giving C = 0.044 mol dm^{-3} for both water and CMC. The concentrations of H^+ and OH^- ions were calculated from the pH after each injection. From these values, as well as C, the concentrations of all the remaining species were calculated for each injection using equations (10), $(14) - (16)$ and (22).

As the conductivity values obtained from the ERT were relative conductivities, these were converted lately to absolute values by multiplying by the initial specific conductivity of the solution of water and CMC respectively 0.0953 mS cm^{-1} and 0.545 mS cm^{-1}. Subsequently, by using the ERT readings as the closest to the true conductivity of the solution, a comparison was drawn between the ERT and the conductivity meter in term of the overall absolute trend (see Figure 1). The percentage difference and the root mean square error (RMSE) were calculated.

Data analysis

Data pre-processing: average, coefficient of variation and mixing time

The data from the ERT measurements consisted of 119880 frames for water and 150350 frames for CMC. For each frame, conductivity was measured for all 316 pixels in each plane, resulting in a total of 37.9 x 10^6 and 47.5 x 10^6 conductivity values for each plane for water and CMC respectively. The data was then exported to MATLAB, where the results were plotted and evaluated.

In order to quantify the degree of difference between the conductivities of the pixels within both planes, the standard deviation was calculated for each frame. However, due to the average conductivity value varying greatly between certain frames (overall changes of absolute conductivity due to injections), in order to standardise the deviation and allow comparisons to be made, the standard deviation was divided by the mean value for each frame, giving the *coefficient of variation* (CoV).

For determining the *mixing time*, the variation was evaluated. It was assumed that a significant increase in variation was indicative of an injection, with a subsequent significant decrease in variation until reaching a stable value indicating satisfactory mixing, due to homogeneity of conductivity across all pixels. The number of frames between these two points was found, and this was subsequently translated into the amount of time taken for mixing to occur. This was achieved using the "*peakfinder"* function in MATLAB, which quickly finds local peaks and valleys (local extrema of the peak) in a noisy vector using a user defined magnitude threshold which corresponded to a 99% mixing time.

In addition, for the analysis of the ERT results on a local basis, the relative conductivity and the CoV collected on the upper of the two planes (Plane 1) were examined as a function of the time between two injections. Selected snapshots of normalized conductivity maps were also observed, in order to gain a detailed view of the time evolution of the local variations due to the additions of the acid and the base in a section of the stirred tank. The conductivity was normalized for comparing the variations with respect to the same initial and final values. For this reason the following normalization of the local relative conductivity C_i is considered:

$$x_i = \frac{C_i - C_{min}}{C_{max} - C_{min}}$$

where C_{min} and C_{max} are the minimum and maximum value achieved by the conductivity, respectively. For the acid addition, the minimum conductivity corresponds to the beginning of the considered time interval, while for the base addition it corresponds to the end and the reverse holds true for the maximum conductivity value.

Data post-processing: regression learner

Supervised machine learning was utilised to produce a model to predict a pH value from an input of conductivity. This process was attempted in three stages (approaches);

-Stage I: training ERT data using directly pH data

The first machine learning simulation used only the ERT and pH data for each injection, shown in Table 1 and 2, resulting in 34 and 41 distinct data points for conductivity and pH for water and CMC respectively. This was done with the aim of finding a strong function that linked conductivity and pH. A believed occurring limitation was the uneven amount (in time) of data between ERT data (1/62.5 s) and pH (one per injection, ~30 s). Computationally it was the less expensive.

-Stage II: training ERT data using pH data extrapolated from curve fitting

It was assumed that using more data samples (matching the time scales) would help the algorithm to learn better and thus produce a more accurate model. In order to generate this additional data, the original ERT and pH data was exported into the curve fitting toolbox in MATLAB. The toolbox then produced a polynomial function which best fitted all of the data samples; this function was then employed to produce 1000 conductivity data samples each for water and CMC. This data was subsequently transferred into the regression learner application for training.

-Stage III: training ERT data coupling with reaction equations

The final testing used the ERT conductivity and the reaction equations which provide the required information to the model in terms of ions concentration at different time step. This of course was achieved providing the cumulative amounts of acid and base added. To combine the molar mass of the different ions and their specific conductivities, the values reported in Table 1 have been used to calculated overall conductivity of the solution at given concentrations of the different species.

Table 1: Equivalent conductivity of electrolytes in aqueous solution for the different ions.

Ions	***Equivalent conductivity of electrolytes in aqueous solution (S cm^2mol^{-1})***
$H^2PO_4^-$	36
HPO_4^{2-}	57
PO_4^{3-}	92
K^+	73
OH^-	198
H^+	349

For each stage, the data are divided in three datasets for the assessment:

(i) A training dataset, consisting in 60% of the acquired data, was fed to the machine for the training process, together with their own corresponding class of belonging.

(ii) A cross-validation dataset, consisting in 20% of the acquired data, used for selecting the optimum number of used features.

(iii) A test dataset, consisting in the remaining 20% of the data, unseen by the machine was used to evaluate the final accuracy of the method.

The process of training and testing the machine learning algorithm is repeated for ten times, where for each repetition, the datasets included in the training and testing are randomly selected. This is done to avoid bias in evaluating the algorithm. The reported results are the average values obtained in the ten repletion steps.

For each stage, a similar workflow for the training of the regression model in the Regression learner has been used. The main steps of this processes are:

1- Choose Regression model Options
2- Training of the Regression Model.
3- Assessing the regression model performance
4- Export Regression model of interest

The regression learner contained 20 different algorithms for regression which could be tested, ranging from support vector machines to Gaussian processes.

The regression learner app automatically train a selection of different models on the given data. A selection of model types, where selected including the most common ones like, linear regression, regression trees, support vector machines (SVM), Gaussian process regression (GPR) and ensembles of trees. The first three (only if SVM has a linear kernel) usually have an easier interpretability compared to the last two. The five models have then being tested with different kernels such as linear, quadratic, cubic and for each model more than one type linear or quadratic kernel, for example can exist.

All 20 different algorithms were utilised for each run, with the output model exhibiting the lowest RMSE being the one chosen. Given the reasonable overall size of the data we selected the option “All” and we selected the model of interest only on the base of the training performance.

The main differences among the models are:

Generally, linear regression models have predictors that are linear in the model parameters, are easy to interpret and are fast for making predictions. These characteristics make linear regression models popular models to try first. However, the highly constrained form of these models means that they often have low predictive accuracy.
Regression trees are easy to interpret, fast for fitting and prediction, and low on memory usage. Regression SVMs are easy to interpret, but can have low predictive accuracy. Nonlinear SVMs are more difficult to interpret, but can be more accurate.
GPR models are often highly accurate, but can be difficult to interpret.
Finally, ensemble models combine results from many weak learners into one high-quality ensemble model. In this case boosted trees and bagged trees have been employed.

3.0 Results and discuss

Analysis of the conductivity variations over space and time

The time evolution of the effect of the acid addition on the average value of the relative conductivity on Plane 1 and of the CoV between the additions 4 and 5 is shown in Figure 2. To be noticed, the recording of the data were done continuously, hence the time t=0 of the following plots is the same for all plots, being the beginning of the experiment prior to any injection.

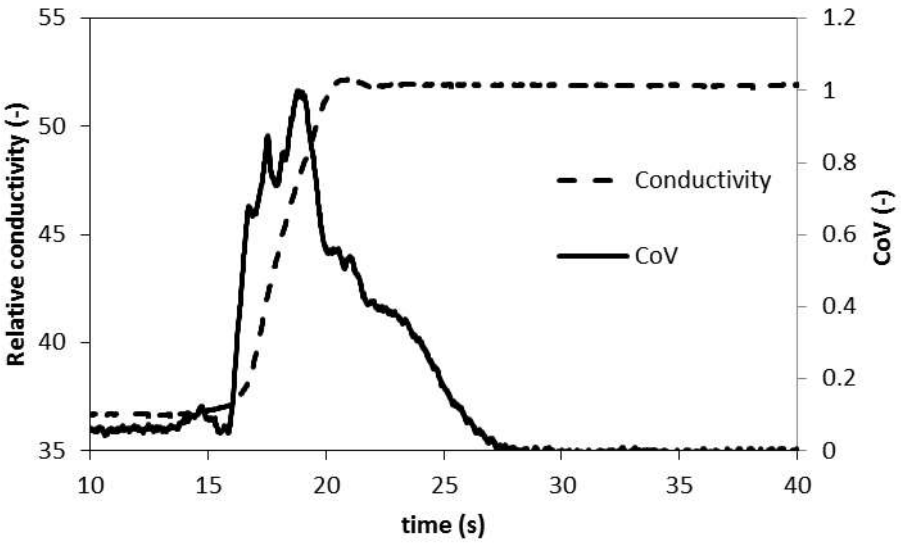

Figure 2. Time trace of relative conductivity and CoV of the local conductivity as a function of time. Acid addition in water (4th injection).

As can be observed, the relative conductivity shows the expected increase up to a constant value. The average constant value of conductivity is achieved after about 5 seconds from the initial detection of the acid on the measurement plane that corresponds to a step increment of the initial conductivity. Besides, the CoV curve provides a closer inspection of the local differences of the conductivity, that achieve a maximum value with a much steeper increase than the decrease down to a constant nil value, that is achieved about 5-6 seconds after that observed from the conductivity curve. It is worth observing that such a difference is not detected in the case of the addition of a passive tracer (Paglianti et al., 2017). The spatial distribution of the normalized conductivity on the two measurement planes is shown in Figure 3 at selected snapshots. Starting from homogeneous conditions at 16 s, the progress of the local increase of conductivity is visible at 18.5 s and 20.5 s and the accomplishment of the acid mixing and dilution is achieved at 22.5 s.

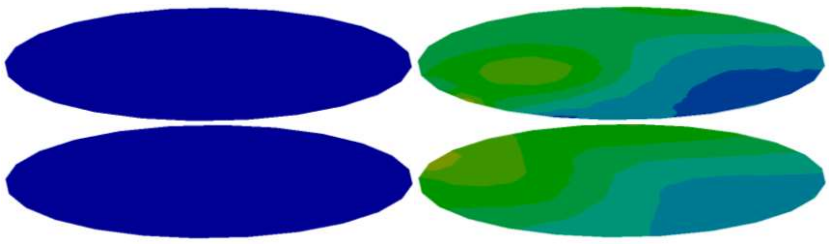

A B

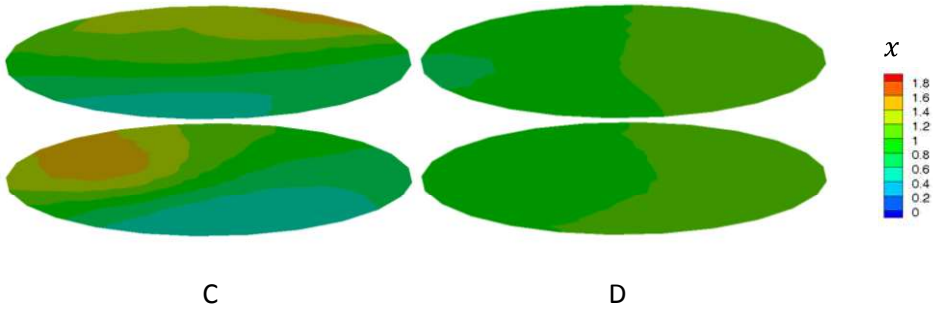

Figure 3. Maps of normalized conductivity on the two measurement planes after the 4th injection of acid in water. A: t=16 s, B: t=18.5 s, C: t=20.5s, D: t=22.5s

A similar representation of the data relevant to the base addition is provided in Figures 4 and 5, where the time interval just after the addition 8 and just before the addition 9 is considered. In this case the trend of the curves shown in Figure 4 is more complex, due to the interaction of different effects proving different contributions to the conductivity variation.

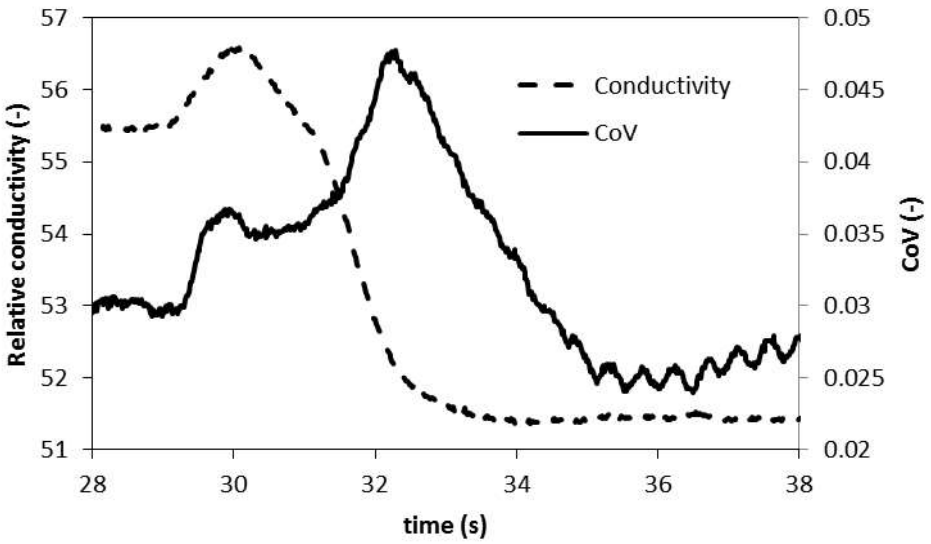

Figure 4. Time trace of relative conductivity and COV of the local conductivity as a function of time. Base addition in water (8th injection).

The conductivity trend is not monotonic due to opposite effects: the increment of the local conductivity, due to the local increase of ions concentration and temperature, related to the heat of dilution and the reduction of the conductivity due to the reaction that reduces the ions concentration. These two effects give rise to two different peaks in the CoV trend.

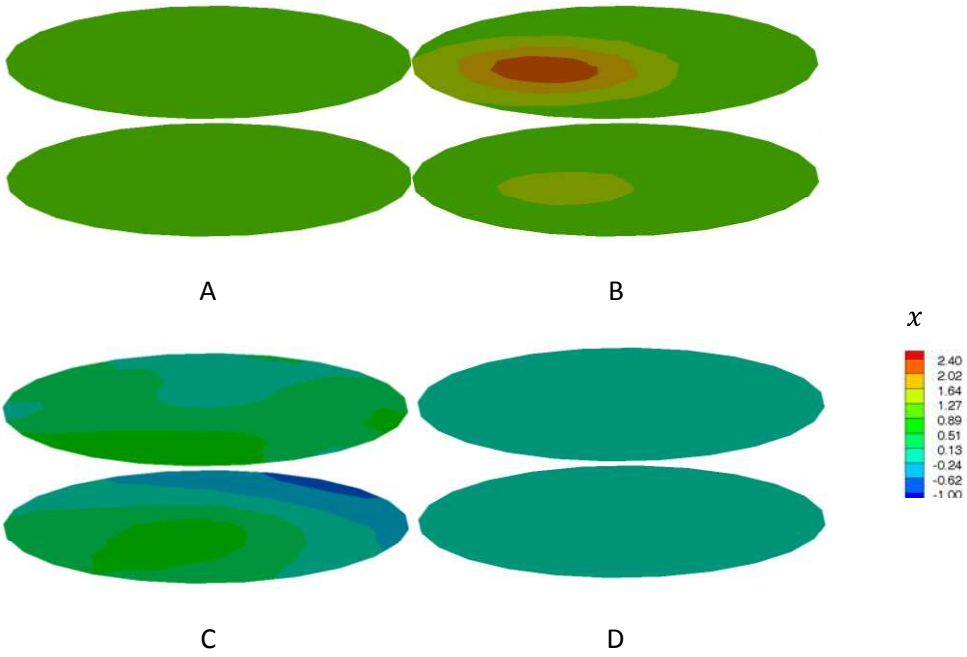

Figure 5. Maps of normalized conductivity on the two measurement planes after the 8th injection of base in water. A: t=28 s, B: t=30 s, C: t=32s, D: t=36s.

Parameter trends over time

The trends of the measured and calculated parameters from the whole set of experimental data are shown in Figure 6. The single points of ERT conductivities have been calculated taking a temporal average between the average between plane 1 and plane 2. This was calculated from 2 seconds of measurement (125 frames per plane) and after a transient steady state was reached, hence a fully mixed system was obtained. Moreover, those conductivities are the mean values of the whole tomogram values. The calculated relative conductivity was then converted to the absolute conductivity as described above in the material and method section in the analytical data paragraph.

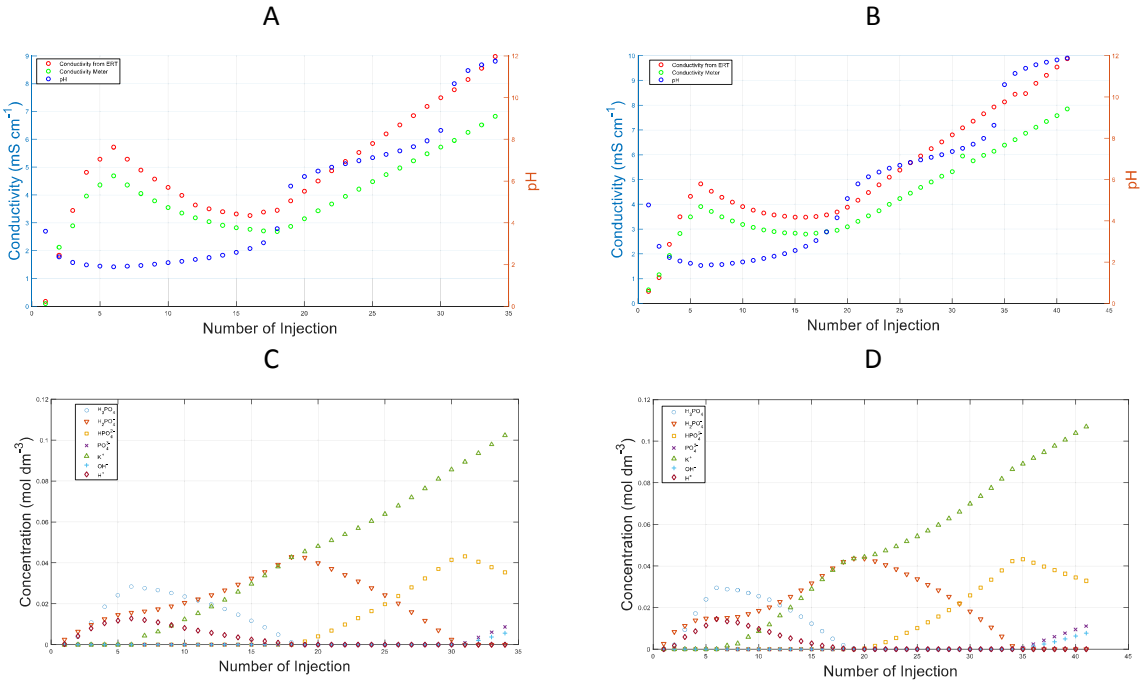

Figure 6. *Graphs showing the trends of ERT, conductivity meter readings, and pH for water (A) and CMC (B), as well as the computed concentration of each species for water (C) and CMC (D).*

For both CMC and water, the pH shows initial decline, and then begins to increase after injection 7, which is when the potassium hydroxide starts to be added. The increase is neither linear, nor it is apparent that it is following a particular function. Instead, the increase is unpredictable, with alternating periods of increasing and decreasing gradient. The shapes of both pH graphs are nearly identical, with the slight differences likely exacerbated by CMC having 41 injections, whereas water had 34.

Looking at the conductivity, the shapes of the two methods are very similar. Initially, there is an increase in conductivity with each injection, up until the point where phosphoric acid ceases to be added and potassium hydroxide begins to be added, where the conductivity begins to decline. The decline continues until approximately injection 17 for both ERT and the conductivity meter, for both water and CMC. After this point, the conductivity begins to increase again with each injection.

As shown in Figure 6 C and D, the water and the CMC graphs for concentration exhibit almost identical characteristics, as expected, with very similar shapes, proportions between the species and concentration values. Initially, there are only three species present with notable concentrations: H_3PO_4, $H_2PO_4^-$ and H^+. The concentration of H_3PO_4 and H^+ continue to increase until injection 7, whereby they begin to decrease due to the constant addition of KOH. K^+ begins to appear at injection 7, where the injection of KOH begins, and it continues to increase constantly throughout the whole experiment, due to constant injections. An interesting observation is that as the concentration of $H_2PO_4^-$ begins to decrease, the concentration of HPO_4^{2-} begins to increase, at approximately the same rate. Likewise, when the concentration of HPO_4^{2-} begins to decrease, the concentration of PO_4^{3-} begins to increase, also at a very similar rate. This shows the commencement of major stages of dissociation of the phosphoric acid derivative species as the pH increases and the concentration of hydrogen ions

decreases. As expected, the concentration of hydroxide ions is very low during periods of high hydrogen ion concentration, with an increase towards the end of the reaction as the solution becomes more basic.

Comparison between conductivity measurements

The comparison of the two conductivity measurements (Figure 6 A and B) shows that both conductivity methods yield results which are similar in shape, though there is a small difference between them, with ERT generally showing higher conductivity readings.

The percentage difference and RMSE between ERT and the conductivity meter is shown in Figure 1. SI and also the % difference between the two measurements. The small discrepancy in conductivity between the ERT and the conductivity meter can be attributed to the fact that the ERT values are an average across all the pixels for both planes, and therefore are representative of the conductivity throughout the whole solution (see Figure 1.SI as reference). In contrast, the conductivity meter measured the conductivity at a single point within the solution where the probe was placed. There is no significant difference between RMSE values for water and CMC.

Comparison of data in the different planes

The ERT conductivity data are shown in Figure 7 A and B, showing the average conductivity for each plane across the range of frames for water and CMC experiment respectively.

A

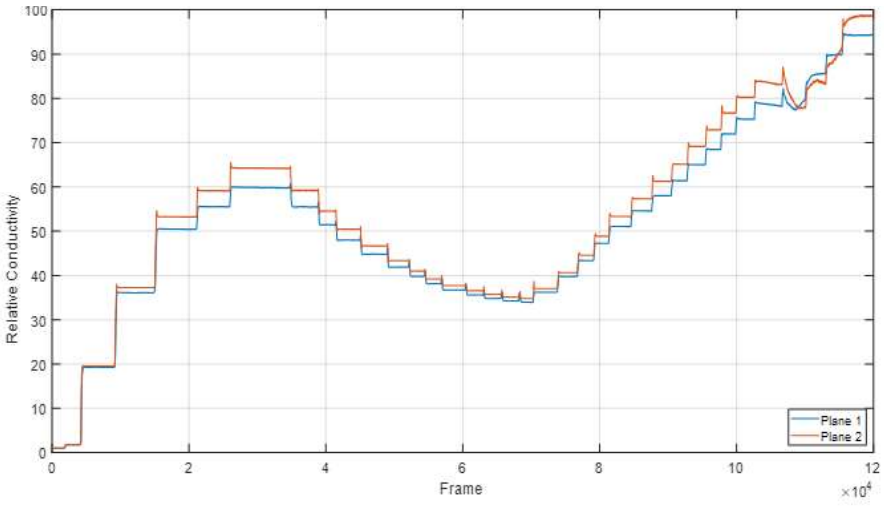

B

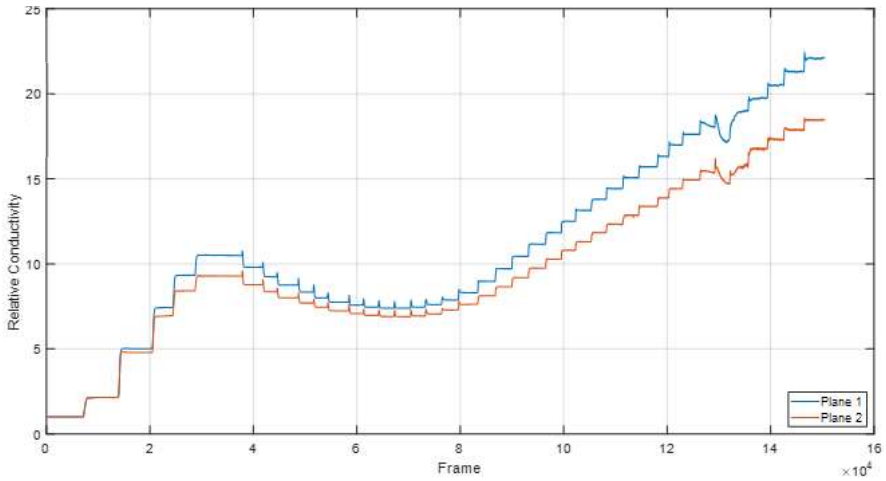

Figure 7. *Average ERT conductivity data for plane 1 and plane 2 for the range of frames for water (A) and CMC (B).*

Examining Figure 7, a few observations can be made about the ERT results. The conductivity fluctuates seemingly at random around a constant value, which is difficult to notice by looking at the graph, but is more apparent when the graph is magnified. The conductivity continues like this until a certain point where it suddenly shows a substantial increase or decrease, this process then repeats itself again. It is evident that these sudden changes in conductivity correspond to the injections of phosphoric acid and potassium hydroxide. It can be seen that the conductivity increases with each addition of phosphoric acid, until potassium hydroxide begins to be added instead, where the conductivity starts to decline with each injection. This decline is only temporary, however, and after a certain number of injections, the conductivity again starts increasing with each addition, with this increase continuing until the conclusion of the experiment. While it may appear strange that the conductivity decreases and then later increases upon the commencement of potassium hydroxide injection, a possible explanation for this could be that hydrogen ions exhibit the highest conductivity out of the ions present in the solution. The addition of potassium hydroxide brings an abundance of hydroxide ions, which inevitably react with and therefore neutralise the hydrogen ions, thus reducing the conductivity of the solution. However, this trend does not continue for long, as ultimately, the conductivity of the solution is determined by the amount and type of ions present, and with each additional injection of potassium hydroxide, the concentration of ions within the solution increases, resulting in an increase in conductivity.

One distinctive feature of the data is a particular period where the conductivity change doesn't show the same behaviour as the others; instead, it demonstrates a slight increase, followed by a decrease which is curved in its shape, and then a subsequent increase. This is in contrast with all of the other injections, which generally show a straight vertical increase or decrease. This phenomenon is demonstrated in both plane 1 and plane 2 and for both mediums, appearing at approximately frame 11 x 10^4 for water and 13 x 10^4 for CMC (injection 30 for water, 35 for CMC both around pH=8). Whilst unusual, upon further examination it was found that this occurs during the injection whereby the

concentrations of both phosphate ions and hydroxide ions suddenly become notable; it is likely that the abrupt increase in presence of these ions affects the conductivity in this peculiar manner.

One interesting observation, upon examining the graphs for water and CMC, is that for water, the conductivity for plane 1 is always similar to plane 2 for the vast majority of frames, whereas for CMC, there is a noticeable difference. This could be explained by the possible different fluid dynamics involved during the blending. In case of turbulent flow, this will minimise the difference between the two planes because mixing within the vessel is more homogenous. The offset between the two planes is mostly influenced by the closer presence of the impeller which slightly perturbs the values of local conductivity in the tomograms of plane 2 (closer to the impeller, see Figure 1). On the contrary, if fluid flow regime is closer to laminar, the overall mixing will be penalised, hence differences will be expected in the two different planes of measurement due to the formation of the pseudo cavern (Adams & Barigou, 2007). For water it is expected a turbulent flow (Reynolds number,Re, within the order of 10^4) whilst for the CMC experiment we are closer to laminar regime (Re within the order of 10).

Mixing time

As described in the material and method paragraph it is possible to evaluate the mixing time of each injection as well as the monitoring of the conductivity in the two measurements planes. Figure 2.SI illustrates how the coefficient of variation, calculated among all pixels for each tomogram, varies with time taking as a reference plane 1.

Each peak indicates an injection, understandably as when acid or base is introduced, there will be areas which will experience higher conductivity relative to other areas of the solution until the vessel is adequately mixed. It can be seen that the earlier injections have a higher variation relative to the others which are due the injection of acid. The variations for water and CMC are mostly similar in their magnitude, with both having the majority of the peaks hovering around the 0.05-0.1 range. There is, however, a difference in how the trend of the coefficient of variation behaves between water and CMC. For water, there doesn't appear to be any particular trend indicating a gradual increase or decrease in the coefficient over time. By contrast, for CMC, it is evident that there is an initial upward trend, followed by a brief downward trend, and then a continuous, gradual upward trend in the variation from approximately frame 7 x 10^4 (frame/total frames=0.46). This is might due to limited mixing efficiency which limits the full dispersion of the chemical species across the entire vessel. The mixing time was subsequently found by determining the number of frames between the beginning and the end of each peak, the results are shown in Figure 8.

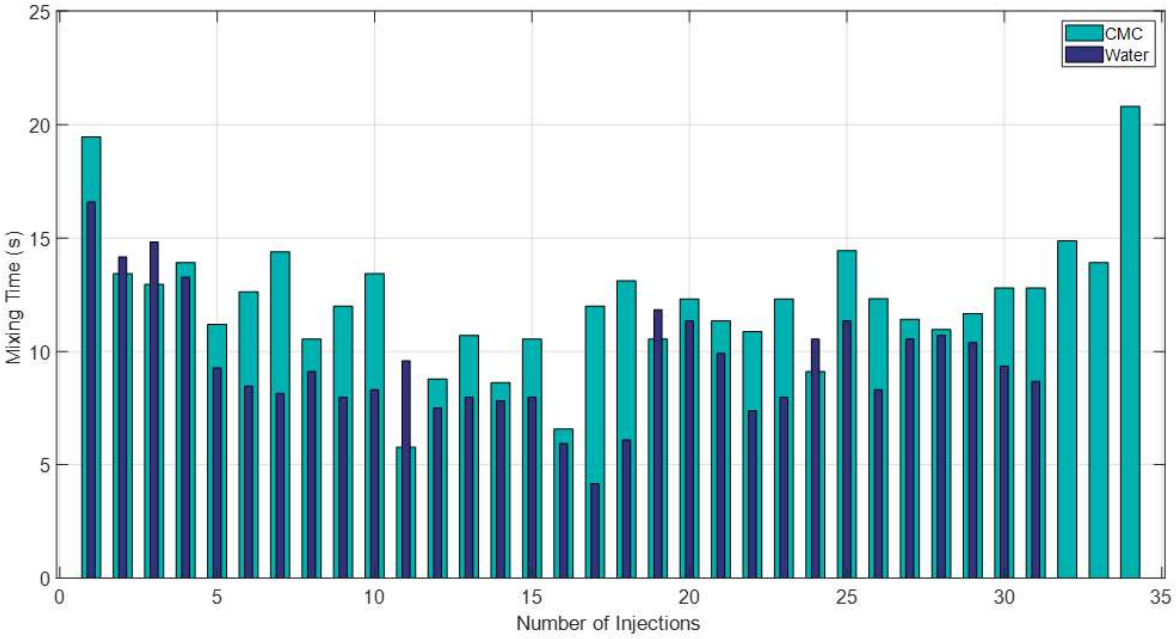

Figure 8. *Mixing time for each injection for water and CMC.*

For the majority of injections, CMC demonstrated a higher mixing time than water. The average mixing time for water across the 31 injections documented was 9.54 seconds, while the average for CMC (across its first 31 injections) was 11.72 seconds. It is worth noticing that with the present working conditions in water, the Grenville and Nienow correlation for the evaluation of mixing time in turbulent non-reacting systems (Grenville & Nienow, 2004) gives a value of 10.9 s. These results are unsurprising, as the more viscous nature of the water and CMC solution compared with just water clearly influences the motion of the fluid by providing more resistance to flow, prolonging the amount of time required for sufficient mixing to occur (Benchabane & Bekkour, 2008), which has been discussed above.

Regression learner

-Stage I: training ERT data using directly pH data

Using the ERT and pH values for each injection, as shown in Table 1.SI and 2.SI, resulted in a model that would require an input of the conductivity, and then give a corresponding pH as an output. The algorithm was trained with the experimental data and 20 different algorithms have been tested, with the best algorithms for water and CMC being:

- Water - Best algorithm: Decision Tree (Fine Tree), RMSE = 1.4418
- CMC - Best algorithm: Gaussian Process Regression (Exponential GPR), RMSE = 1.0353

The RMSE is calculated between the actual pH and the predicted pH of the model.

The Decision Tree algorithm uses a tree model to continuously split and categorise the data until an output is reached, it essentially uses nested if-else conditions. The Fine Tree is one of three tree

algorithms, the other two being Course Tree and Medium Tree, within MATLAB's regression learner. It is characterised by having a high model flexibility, with a high number of maximum splits (100) relative to the other tree algorithms. Gaussian Process Regression models are non-parametric, kernel-based models; exponential GPR uses an exponential kernel, hence more difficult to mathematically interpret.

Evidently, the algorithm for CMC produces a model with a more accurate fit than the one for water, indicated by the lower RMSE. However, when considering the fact that the pH for this experiment was typically between 2 and 12, RMSE values of 1.4418 and 1.0353 are incredibly high. This indicates that using only the ERT conductivity and pH values for each injection as the sole data for machine learning does not result in an accurate predictive model.

-Stage II: training ERT data using pH data extrapolated from curve fitting

Figure 3.SI shows the curve fitted data using MATLAB's curve fitting toolbox to generate polynomials for the ERT conductivity and the pH. All of the curves are fitted in a high order polynomials (9^{th}) as these were found to give a better fit than smaller order polynomials. This lead to polynomials as function y=f(x), where y is the conductivity or the pH, and x is the number of injections. Although in reality, neither are functions of the number of injections, this was used merely to generate the required data sample. Subsequently, 1000 input values of x were used, from 1 to 34 for water and 1 to 41 to CMC, in order to generate 1000 values of the conductivity and the pH.

These values were input, as before, into the regression learner, with conductivity as the input and pH as the output. The results comparing the actual pH and the predicted pH are shown in Figure 9.

A

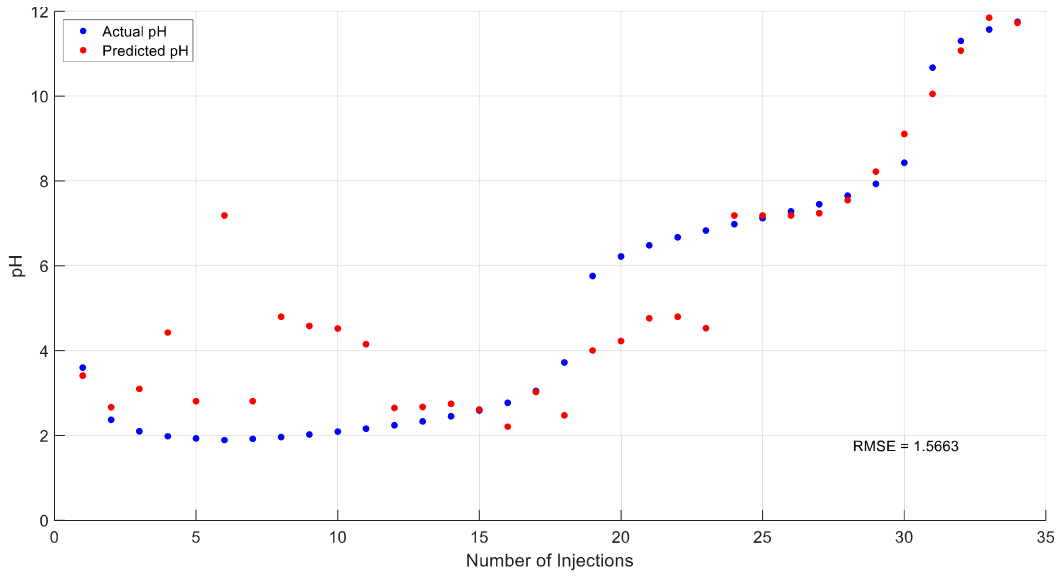

B

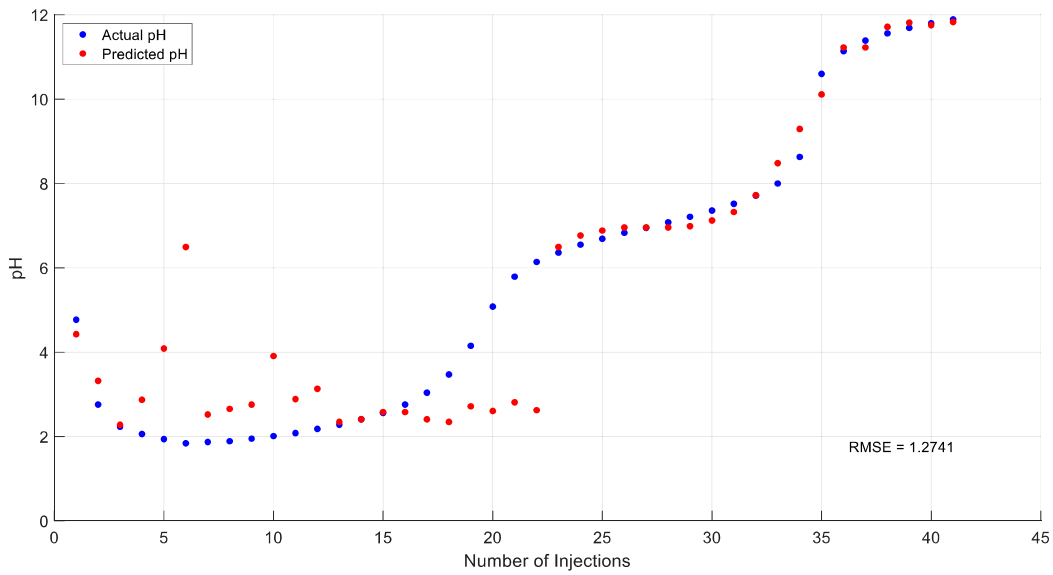

Figure 9. *Machine learning predicted pH (red) and actual pH (blue) for water (A) and CMC (B) from models using curve fitted data as training variables for the algorithm.*

The best algorithm for both was exponential GPR. From Figure 9, it is apparent that even still, the model performs poorly with predicting the pH from the conductivity. This is especially true for the injections at the beginning and the middle, which are characterised by the predicted pH shown in red being significantly different to the actual pH in blue. After roughly injection 24 for water and 23 for CMC, however, the predicted and the actual pH are much closer together, although there is still a noticeable error.

The RMSE between the predicted and curve fitted pH was 1.3212 and 0.91871 for water and CMC respectively, which are better RMSE values than using just the experimental data (1.4418 and 1.0353), understandably, as a larger data set was used. However, after using the model for the actual ERT values and then producing the predicted pH values, the RMSE became 1.5663 and 1.2741 for water and CMC respectively. These RMSE values are higher than the results showed for stage I. This might due to the use of high order polynomial for the regression. However, the use of lower order polynomial would increase consistently the error on the actual pH and conductivity values. Thus, this was not considered giving a very high discrepancy in the input values of the model. Therefore, using curve fitting for the generation of more data samples did not improve the model, and instead made it less accurate. Despite the negative outcome this was an important lesson for a practical use of ML techniques. The amount of data to provide to the learner is important but not always quantity is the right approach. Quality and how an information can enrich the learning is often more relevant.

-Stage III: training ERT data coupling with reaction equations

Finally, as discussed in the material and method section for the stage III, the regression learner inputs where the conductivity and the amount of acid or base added to the system (amounts in volume of each injections). The equations described by equations (10), (14-16), (22)- where integrated in the model. In Figure 10, the results of the actual and the predicted pH are shown.

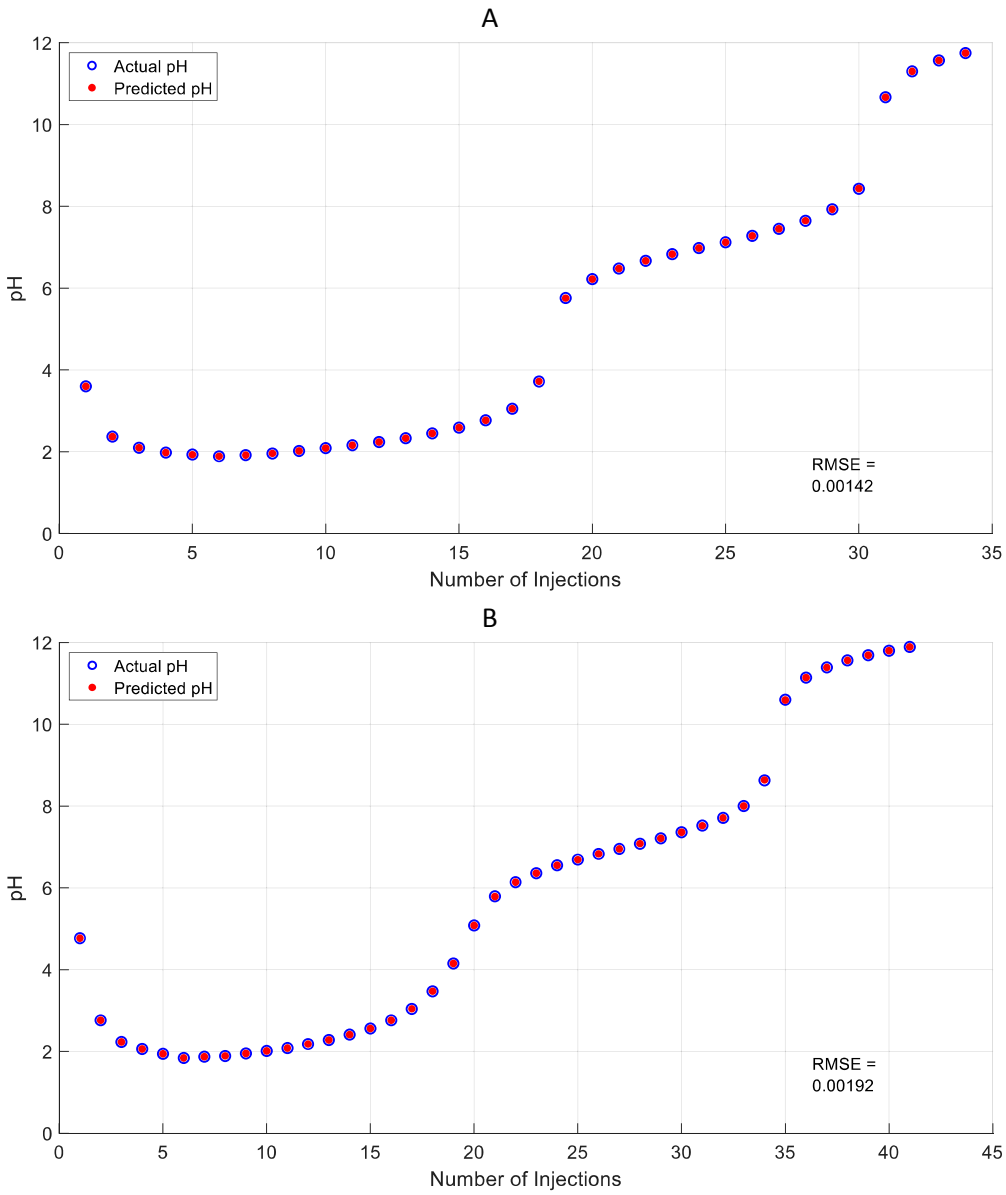

Figure 10. *Machine learning predicted pH (red) and actual pH (blue) for water (A) and CMC (B) from models using ERT conductivity, amount of acid, and amount of base as inputs for the algorithm.*

Figure 10 shows an almost perfect prediction of pH by the model, evident by the scatter points essentially being in the same locations, which is highlighted by the significantly low RMSE values of 0.00142 and 0.00192 for water and CMC respectively. The best algorithm which was used to produce these models was exponential GPR.

Using this model, a high frequency measurement of the pH from ERT data was achieved and it as shown in Figure 11.

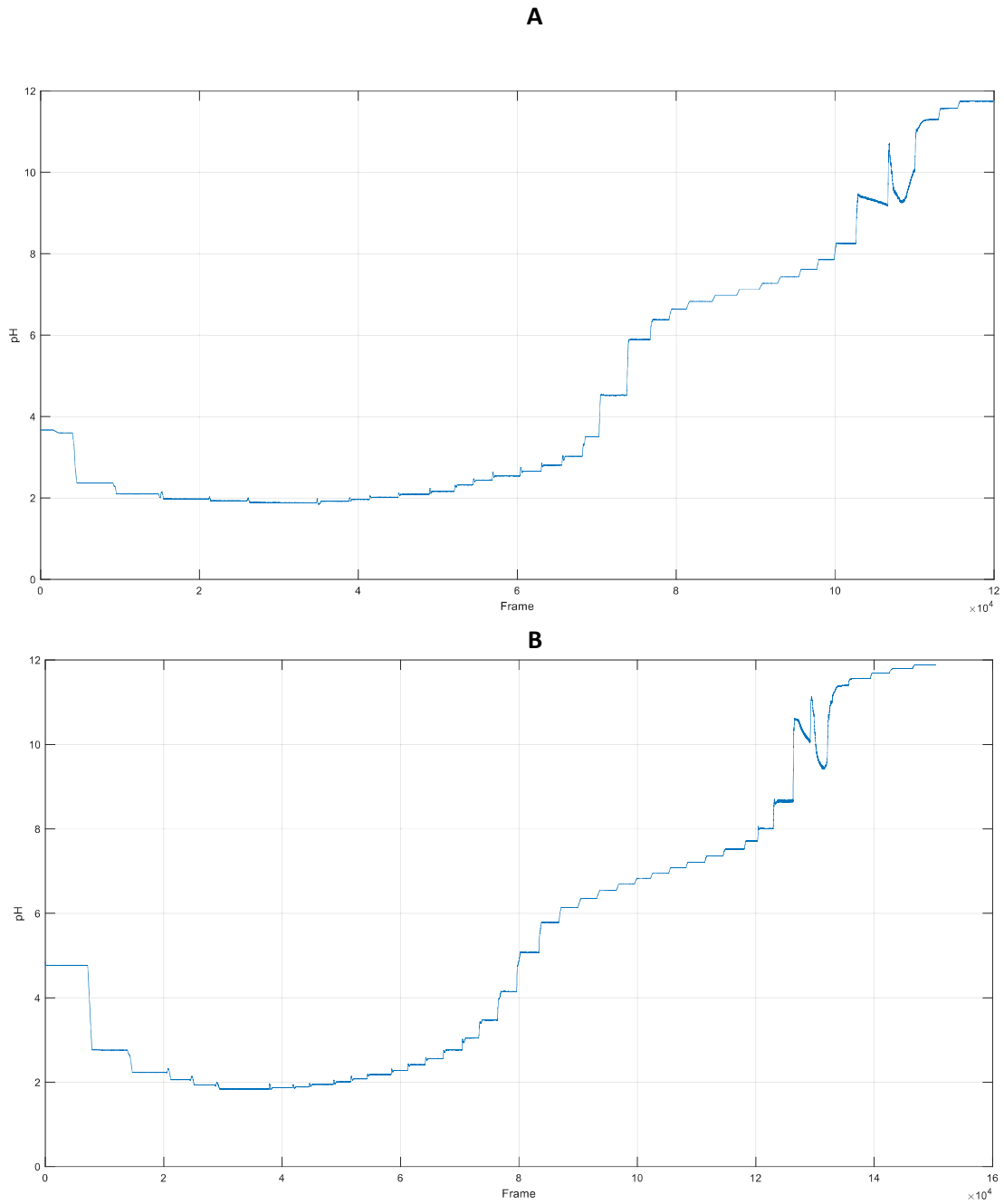

Figure 11. *pH values for each frame for water(A) and CMC (B) obtained from ERT measurements.*

Figure 11 shows the average pH across all pixels for every single frame for the duration of the experiment. This enables the pH to be monitored closely and precisely at each moment in time. One challenge, however, is that the pH is likely to be less accurate during the injection and while is approaching a new steady state (practically, during the mixing times which range between ~5 to 20 s, from the actual injection to reach the new steady state as shown in Figure 7 and 2.SI). This is due to the more discrete nature of the injections as opposed to the continuous conductivity data and ideally those should have the same nature being both inputs of the same model. To account for it, the amount of acid or base was considered added in equal volumes in time (similar to a pulse change) instead of

considering a step change (as the injections actually were) over the different mixing times (for each injection). This model assumes a steady state well mixed system which does not allow the precise determination of transient pH during the mixing stages of each injection. This is particularly challenging also due to local thermal effect (due to reaction) and our assumption of well mixed/steady state cannot be supported.

4.0 Conclusions

The use of ERT for monitoring the reaction between phosphoric acid and potassium hydroxide in mediums of both water and CMC solution was assessed. It was found that the conductivity values obtained from ERT can be used to visualise the progress of the reaction and determine exactly when new additions of acid or base were introduced through sharp increases or decreases in conductivity.

Analysis of the variation of conductivity between the pixels within both planes enabled the determination of the mixing times for each injection of acid and base. The subsequent values for mixing time indicated CMC having a higher average mixing time than water, owing to it being the more viscous fluid.

The usage of machine learning to develop a model that could effectively serve as a function to produce an output of pH from an input of ERT yielded mixed results. Using experimental data of ERT conductivity and pH for the training of the algorithm resulted in a very inaccurate model. Curve fitting was used to generate more training data, resulting in an even more inaccurate model. Finally, the use of the ERT data in conjunction with the cumulative quantities of acid and base as input variables resulted in very accurate models, which were subsequently used to produce a continuous plot of pH over the course of the reaction.

Furthermore, as the concentrations of the species of the reaction can be directly determined from the pH, real-time monitoring of concentrations could also be achieved. The nature of ERT also allows these measurements to be taken across the whole plane, as well as individual pixels, allowing the close monitoring of different regions of the fluid. This would serve to be very useful, particularly with reaction vessels of a considerable size.

Acknowledgements

Daniel Bezchi was a MEng student from the school of Chemical Engineering of the University of Birmingham which carried out the post-processing work of the experimental data using MATLAB.

Irene Mannino was a visiting student at the University of Birmingham from the Dipartimento di Chimica Industriale of the University of Bologna funded by Erasmus + scholarship academic year 2018/2019. She carried out part of the experimental work.

On behalf of all authors, the corresponding author states that there is no conflict of interest.

References

Adams, L. W., & Barigou, M. (2007). CFD analysis of caverns and pseudo-caverns developed during mixing of non-Newtonian fluids. *Chemical Engineering Research and Design*, *85*(5 A), 598–604. https://doi.org/10.1205/cherd06170

Bantscheff, M., Schirle, M., Sweetman, G., Rick, J., & Kuster, B. (2007). Quantitative mass spectrometry in proteomics: A critical review. *Analytical and Bioanalytical Chemistry*, *389*(4), 1017–1031. https://doi.org/10.1007/s00216-007-1486-6

Barber, C. C., & Brown, B. H. (1983). Imaging spatial distributions of resistivity using applied potential tomography. *Electronics Letters*, *19*(22), 933–935. https://doi.org/10.1049/el:19830637

Benchabane, A., & Bekkour, K. (2008). Rheological properties of carboxymethyl cellulose (CMC) solutions. *Colloid and Polymer Science*, *286*(10), 1173–1180. https://doi.org/10.1007/s00396-008-1882-2

Bowler, A. L., Bakalis, S., & Watson, N. J. (2020). A review of in-line and on-line measurement techniques to monitor industrial mixing processes. *Chemical Engineering Research and Design*, *153*, 463–495. https://doi.org/10.1016/j.cherd.2019.10.045

Carletti, C., Montante, G., Westerlund, T., & Paglianti, A. (2014). Analysis of solid concentration distribution in dense solid-liquid stirred tanks by electrical resistance tomography. *Chemical Engineering Science*, *119*, 53–64. https://doi.org/10.1016/j.ces.2014.07.049

Clarke, S. M., Griebsch, J. H., & Simpson, T. W. (2005). Analysis of support vector regression for approximation of complex engineering analyses. *Journal of Mechanical Design, Transactions of the ASME*, *127*(6), 1077–1087. https://doi.org/10.1115/1.1897403

Dickin, F., & Wang, M. (1996). Electrical resistance tomography for process applications. *Measurement Science and Technology*, *7*(3), 247. https://doi.org/10.1088/0957-0233/7/3/005

Edwards, I., Axon, S. A., Barigou, M., & Stitt, E. H. (2009). Combined use of PEPT and ERT in the study of aluminum hydroxide precipitation. *Industrial and Engineering Chemistry Research*, *48*(2), 1019–1028. https://doi.org/10.1021/ie8010353

Forte, G., Albano, A., Simmons, M. J. H., Stitt, H. E., Brunazzi, E., & Alberini, F. (2019). Assessing Blending of Non-Newtonian Fluids in Static Mixers by Planar Laser-Induced Fluorescence and Electrical Resistance Tomography. *Chemical Engineering and Technology*, *42*(8), 1602–1610. https://doi.org/10.1002/ceat.201800728

Forte, G., Alberini, F., Simmons, M. J. H., & Stitt, E. H. (2019). Measuring gas hold-up in gas–liquid/gas–solid–liquid stirred tanks with an electrical resistance tomography linear probe. *AIChE Journal*, *65*(6), e16586. https://doi.org/10.1002/aic.16586

Gradov, D. V., González, G., Vauhkonen, M., Laari, A., & Koiranen, T. (2018). Experimental investigation of reagent feeding point location in a semi-batch precipitation process. *Chemical Engineering Science*, *190*, 361–369. https://doi.org/10.1016/j.ces.2018.06.042

Grenville, R. K., & Nienow, A. W. (2004). Blending of Miscible Liquids. In *Handbook of Industrial Mixing* (pp. 507–542). John Wiley & Sons, Inc. https://doi.org/10.1002/0471451452.ch9

Hastie, T., Tibshirani, R., & Friedman, J. (n.d.). *Springer Series in Statistics The Elements of Statistical Learning Data Mining, Inference, and Prediction*.

Hosseini, S., Patel, D., Ein-Mozaffari, F., & Mehrvar, M. (2010). Study of solid-liquid mixing in agitated tanks through electrical resistance tomography. *Chemical Engineering Science*, *65*(4), 1374–

1384. https://doi.org/10.1016/j.ces.2009.10.007

Jiao, Z., Hu, P., Xu, H., & Wang, Q. (2020). Machine learning and deep learning in chemical health and safety: A systematic review of techniques and applications. In *Journal of Chemical Health and Safety* (Vol. 27, Issue 6, pp. 316–334). American Chemical Society. https://doi.org/10.1021/acs.chas.0c00075

Kagoshima, M., & Mann, R. (2005). Interactions of precipitation and fluid mixing with model validation by electrical tomography. *Chemical Engineering Research and Design*, *83*(7 A), 806–810. https://doi.org/10.1205/cherd.04338

Kazemzadeh, A., Ein-Mozaffari, F., Lohi, A., & Pakzad, L. (2016). A new perspective in the evaluation of the mixing of biopolymer solutions with different coaxial mixers comprising of two dispersing impellers and a wall scraping anchor. *Chemical Engineering Research and Design*, *114*, 202–219. https://doi.org/10.1016/j.cherd.2016.08.017

Khajeh Naeeni, S., & Pakzad, L. (2019). Experimental and numerical investigation on mixing of dilute oil in water dispersions in a stirred tank. *Chemical Engineering Research and Design*, *147*, 493–509. https://doi.org/10.1016/j.cherd.2019.05.024

Lee, J. H., Shin, J., & Realff, M. J. (2018). Machine learning: Overview of the recent progresses and implications for the process systems engineering field. *Computers and Chemical Engineering*, *114*, 111–121. https://doi.org/10.1016/j.compchemeng.2017.10.008

Maluta, F., Montante, G., & Paglianti, A. (2020). Analysis of immiscible liquid-liquid mixing in stirred tanks by Electrical Resistance Tomography. *Chemical Engineering Science*, *227*, 115898. https://doi.org/10.1016/j.ces.2020.115898

Montante, G., & Paglianti, A. (2015). Gas hold-up distribution and mixing time in gas-liquid stirred tanks. *Chemical Engineering Journal*, *279*, 648–658. https://doi.org/10.1016/j.cej.2015.05.058

Paglianti, A., Carletti, C., & Montante, G. (2017). Liquid Mixing Time in Dense Solid-Liquid Stirred Tanks. *Chemical Engineering & Technology*, *40*(5), 862–869. https://doi.org/10.1002/ceat.201600595

Parmar, C., Grossmann, P., Bussink, J., Lambin, P., & Aerts, H. J. W. L. (2015). Machine Learning methods for Quantitative Radiomic Biomarkers. *Scientific Reports*, *5*(1), 1–11. https://doi.org/10.1038/srep13087

Qin, S. J., & Chiang, L. H. (2019). Advances and opportunities in machine learning for process data analytics. *Computers and Chemical Engineering*, *126*, 465–473. https://doi.org/10.1016/j.compchemeng.2019.04.003

Rasmussen, C. E., & De, H. M. (2010). Gaussian Processes for Machine Learning (GPML) Toolbox Hannes Nickisch. In *Journal of Machine Learning Research* (Vol. 11). http://www.kyb.tuebingen.mpg.de/bs/people/carl/code/minimize/.

Rauniyar, N. (2015). Parallel Reaction Monitoring: A Targeted Experiment Performed Using High Resolution and High Mass Accuracy Mass Spectrometry. *International Journal of Molecular Sciences*, *16*(12), 28566–28581. https://doi.org/10.3390/ijms161226120

Sharifi, M., & Young, B. (2013). Electrical resistance tomography (ERT) for flow and velocity profile measurement of a single phase liquid in a horizontal pipe. *Chemical Engineering Research and Design*, *91*(7), 1235–1244. https://doi.org/10.1016/j.cherd.2013.02.004

Sheeba, A., Akhil, R., & Prakash, M. J. (2020). Heat transfer and flow characteristics of a conical coil heat exchanger. *International Journal of Refrigeration*, *110*, 268–276. https://doi.org/10.1016/j.ijrefrig.2019.10.006

Shi, T., Su, D., Liu, T., Tang, K., Camp, D. G., Qian, W. J., & Smith, R. D. (2012). Advancing the sensitivity of selected reaction monitoring-based targeted quantitative proteomics. In *Proteomics* (Vol. 12, Issue 8, pp. 1074–1092). John Wiley & Sons, Ltd. https://doi.org/10.1002/pmic.201100436

St-Gelais, D., Champagne, C. P., Erepmoc, F., & Audet, P. (1995). The use of electrical conductivity to follow acidification of dairy blends. *International Dairy Journal*, *5*(5), 427–438. https://doi.org/10.1016/0958-6946(95)00027-Z

Stamatopoulos, K., Batchelor, H. K., Alberini, F., Ramsay, J., & Simmons, M. J. H. (2015). Understanding the impact of media viscosity on dissolution of a highly water soluble drug within a USP 2 mini vessel dissolution apparatus using an optical planar induced fluorescence (PLIF) method. *International Journal of Pharmaceutics*, *495*(1). https://doi.org/10.1016/j.ijpharm.2015.09.002

Venkatasubramanian, V. (2019). The promise of artificial intelligence in chemical engineering: Is it here, finally? *AIChE Journal*, *65*(2), 466–478. https://doi.org/10.1002/aic.16489

Wabo, E., Kagoshima, M., & Mann, R. (2004). Batch stirred vessel mixing evaluated by visualized reactive tracers and electrical tomography. *Chemical Engineering Research and Design*, *82*(9 SPEC. ISS.), 1229–1236. https://doi.org/10.1205/cerd.82.9.1229.44159